PAPER

Optimized aperiodic broadband visible absorbers

IOP Publishing Journal of Optics
J. Opt. 19 (2017) 105003 (7pp) https://doi.org/10.1088/2040-8986/aa8673

Optimized aperiodic broadband visible absorbers

Christopher H Granier[1], Simón G Lorenzo[1,2], Chenglong You[1], Georgios Veronis[2,3] and Jonathan P Dowling[1]

[1] Hearne Institute for Theoretical Physics, Department of Physics and Astronomy, Louisiana State University, Baton Rouge, LA 70803, United States of America
[2] Center for Computation and Technology, Louisiana State University, Baton Rouge, LA 70803, United States of America
[3] School of Electrical Engineering and Computer Science, Louisiana State University, Baton Rouge, LA 70803, United States of America

E-mail: cyou2@lsu.edu

Received 14 February 2017, revised 17 July 2017
Accepted for publication 16 August 2017
Published 27 September 2017

Abstract

We design a visible wavelength range broadband absorber based on an optimized aperiodic structure, which is capable of almost doubling the absorptance in the visible range, in comparison to tungsten. Our optimized structure is either a tungsten-air or a tungsten-silicon carbide multilayer stack on top of a tungsten substrate. We achieve almost perfect impedance matching between this structure and air. We find that the high absorptance is not related to resonances with high quality factors and no field enhancement is observed, which is in agreement with the broadband and broad-angle absorptance of our structure.

Keywords: nanophotonics, physical optics, absorbers

(Some figures may appear in colour only in the online journal)

1. Introduction

The absorptance and emittance of bulk materials, textured structures and other configurations have been intensely investigated in recent history. While bulk absorbers possess isotropic and broadband absorptance spectra, it has been shown that the absorptance of bulk materials can be drastically enhanced even over a broad wavelength range by utilizing specialized geometries, multilayer structures and three-dimensional constructions [1]; possibly in combination with a bulk-material substrate. Broadband absorbers and emitters in the visible and near-infrared wavelength range have been widely researched, due to their many possible applications in conventional photovoltaic and themophotovoltaic solar energy conversion [2, 3], as well as in electro-optical detectors [4–6]. Many structures have been used to achieve near-unity broadband absorptance, including impedance matching structures [7, 8], photonic crystals [9], metamaterials [10–12] and structures supporting multiple resonances [13].

In this paper, we design aperiodic broadband visible absorbers. We first consider tungsten-air multilayer stacks on top of a tungsten substrate as a proof of concept. We next consider tungsten-silicon carbide multilayer stacks. We used a hybrid optimization method, which includes a micro-genetic global optimization method, and a local optimization method, to maximize the absorptance in the visible. We find that the optimized structures obtained using this process show drastically improved absorptance in the visible range in comparison to tungsten. When optimized, these structures exhibit absorptance which approaches unity. In addition, we find that the optimized tungsten-air structure is essentially equivalent to a reduced structure consisting of a thin tungsten layer and an air layer above a thick tungsten substrate. Similarly, we find that the optimized tungsten-silicon carbide structure is essentially equivalent to a reduced structure which consists of a single silicon carbide layer above a thick tungsten substrate.

The remainder of the paper is organized as follows. In section 2, we discuss the computational techniques used. The results obtained using these techniques are presented in

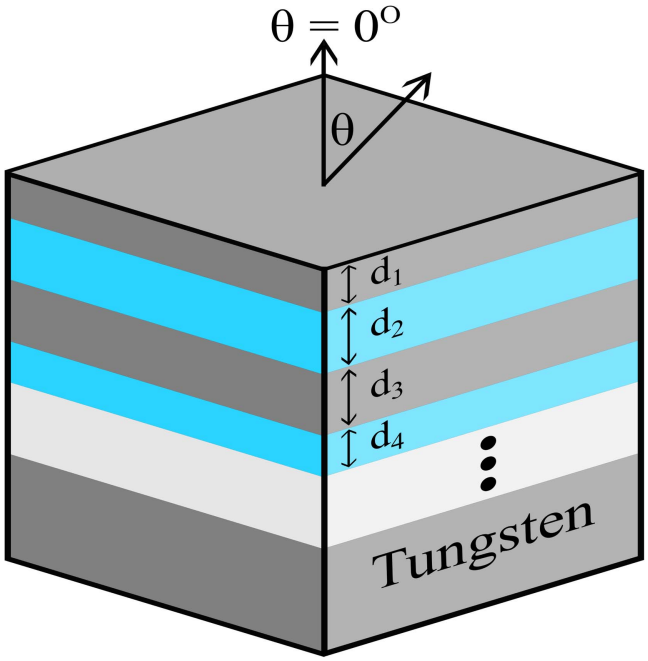

Figure 1. Schematic of the structure optimized. It consists of alternating layers of tungsten and air or tungsten and silicon carbide above a semi-infinite tungsten substrate.

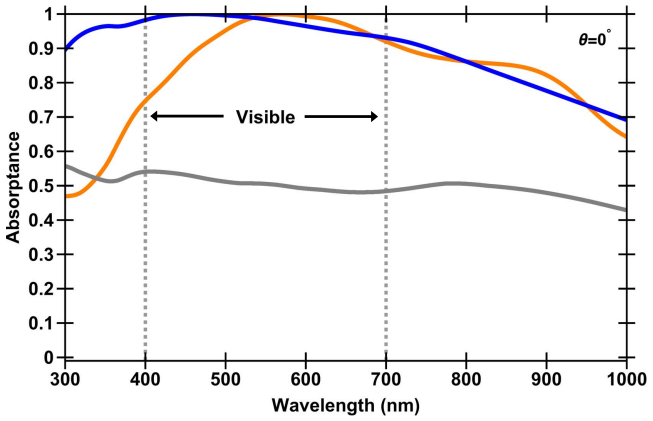

Figure 2. Absorptance in the normal direction, $A(\lambda, \theta = 0°)$, as a function of wavelength for the optimized structures compared to the reference bulk tungsten structure. The gray line shows the performance of bulk tungsten. The orange and blue lines show the performance of the optimized TSiC and TA structures, respectively. The layer thicknesses of the optimized structures, in units of nanometers, beginning with the tungsten layer bordering air are: {3.4, 90, 163, 500} for the TA structure and {0, 39, 66, 319} for the TSiC structure.

section 3. Finally, our conclusions are summarized in section 4.

2. Theory

We model a structure composed of infinite slabs of material of varying aperiodic thicknesses above a semi-infinite tungsten substrate, as depicted in figure 1 [14]. Utilizing the transfer-matrix method [15], we calculate the transmittance, reflectance and absorptance of the structure for both TE and TM polarized light. Light is incident from air at an angle θ to the structure. We make use of experimental data for the wavelength-dependent indices of refraction, both real and imaginary parts, for silicon carbide and tungsten [16] in all calculations done in this paper. Since the tungsten substrate is taken to be semi-infinite, the transmittance is identically zero, so that:

$$A_{\mathrm{TE/TM}}(\lambda, \theta) = 1 - R_{\mathrm{TE/TM}}(\lambda, \theta), \tag{1}$$

where $A_{\mathrm{TE/TM}}$ is the TE/TM absorptance, $R_{\mathrm{TE/TM}}$ is the TE/TM reflectance and λ is the wavelength.

Our reference structure is the structure in figure 1 without any layers on top of the tungsten substrate. Tungsten is highly reflective over the visible wavelength range. Hence, tungsten is a relatively poor absorber, with an average absorptance over the visible spectrum of approximately 50% (figure 2). We define the enhancement factor Q of a given structure compared to our reference structure as the ratio of the average absorptance in the visible in the normal direction to the average absorptance of our reference structure in the normal direction:

$$Q = \frac{\int_{\lambda_1}^{\lambda_2} A(\lambda, \theta = 0°)\, \mathrm{d}\lambda}{\int_{\lambda_1}^{\lambda_2} A_{\mathrm{Bulk}}(\lambda, \theta = 0°)\, \mathrm{d}\lambda}, \tag{2}$$

where $\lambda_1 = 400$ nm and $\lambda_2 = 700$ nm.

3. Results

Our goal is to maximize the average absorptance of the structures in the visible range. We use a hybrid optimization method, which includes a micro-genetic global optimization method [14, 17–23] and a derivative-free local optimization method [24, 25], to find the optimal thicknesses in the multilayer structures.

The genetic algorithm is an iterative optimization method. It starts with a population of structures, which are randomly selected. These gradually evolve towards improved structures, via the application of the genetic operators. These genetic operators are patterned after the natural selection process. In the initialization function, a population of chromosomes is created by a random selection of values for the genes. The genetic algorithm then proceeds to iteratively generate a new population by the application of selection, crossover and mutation operators.

More specifically, here we use a micro-genetic algorithm developed in house. It has been shown that the micro-genetic algorithm avoids premature convergence and shows faster convergence to the near-optimal region compared with the conventional large-population genetic algorithm for multi-dimensional problems [17–19]. The micro-genetic algorithm

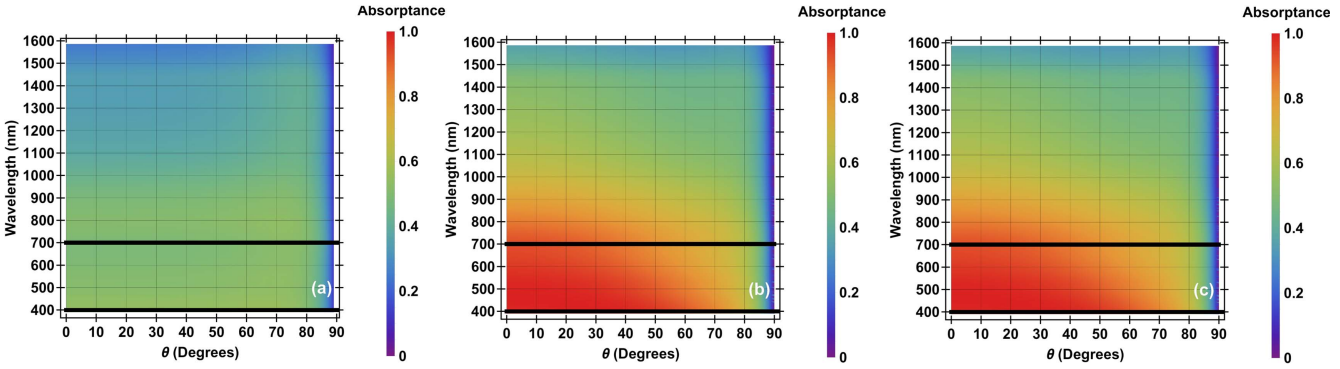

Figure 3. (a) Absorptance of our reference bulk tungsten structure as a function of wavelength and angle. (b) Absorptance of the optimized TA structure as a function of wavelength and angle. (c) Absorptance of the optimized TSiC structure as a function of wavelength and angle. The layer thicknesses of the optimized TA and TSiC structures are given in figure 2. The horizontal, thick, black lines show the visible wavelength range.

starts with a small random population that evolves and converges after a few generations.

Once the population converges, the best individual of the generation is passed on to the local optimization algorithm to find the local optimum. More specifically, here we use the constrained optimization by linear approximations (COBYLA) algorithm for local derivative-free optimization included in a free-software package, which implements several optimization algorithms [24, 25]. This algorithm constructs successive linear approximations of the objective function, and optimizes these approximations in a trust region at each step. The structure obtained from the local optimization algorithm is returned to the micro-genetic algorithm and used in conjunction with new random structures to generate the next population. The process is iteratively repeated. We found that using such a hybrid scheme greatly accelerates the convergence of the optimization algorithm compared to pure genetic optimization algorithms.

We use tournament selection as the selection scheme in the micro-genetic algorithm. In this method, a subpopulation of individuals is randomly chosen from the population and made to compete on the basis of their fitness values. The individual in the subpopulation with the highest fitness value wins the tournament and is thus selected. The remaining members of the entire subpopulation are then put back into the general population and the process is repeated. This selection scheme converges more rapidly and has a faster execution time compared to other competing schemes [20]. Once a pair of individuals is selected as parents, the basic crossover operator creates two offspring by combining the chromosomes of their parents. We use uniform crossover rather than single point crossover, as it has been found that micro-genetic algorithm convergence is faster with uniform crossover [17, 20]. An elitist strategy [21] is also employed, wherein the best individual from one generation is passed on to the next generation.

The fitness function F_1 that we maximize is

$$F_1 = \int_{\lambda_1}^{\lambda_2} A(\lambda, \theta = 0^\circ)\, \mathrm{d}\lambda. \tag{3}$$

Our goal is maximize the absorptance over the visible wavelength range.

We investigate four-layer tungsten-air (TA) or tungsten-silicon carbide (TSiC) stacks on top of a tungsten substrate (figure 1). We found that using more than four layers leads to a negligible improvement to the structures performance. The absorptance of the four-layer stacks is optimized with the procedure described above (equation (3)).

Both the TA- and TSiC-optimized structures that we obtained using this process almost double the average absorptance in the visible range, in comparison to tungsten (figure 2). When optimized, these structures exhibit absorptance which approaches unity. We observe that both the TA (figure 3(b)) and TSiC (figure 3(c)) optimized structures lead to drastically increased absorptance in the visible in comparison to tungsten (figure 3(a)). The enhancement factors Q (equation (2)) of the optimized TA and TSiC structures are given in table 1.

Figure 4(a) shows the electric field amplitude profile for the optimized TA structure. The field amplitude is normalized with respect to the incident plane wave field amplitude. The plane wave is normally incident and has a wavelength of $\lambda = 550$ nm. The reflectance of the TA structure is only $\sim$10%, since almost perfect impedance matching between the structure and air is achieved. Additionally, the field in the structure is not enhanced. Therefore, the high absorptance is not due to strong resonances, in other words, the quality factor of the resonances is low. This is in agreement with the broadband and broad-angle absorptance of the structure (figure 3(b)).

We also consider the effect of individual layer thicknesses on the absorptance spectra of the TA structures (figures 5(a) and (b)). The optimized thickness of the tungsten layer adjacent to air is found to be 3.4 nm, due to the fact that a thinner tungsten layer does not achieve near-perfect absorptance in the visible wavelength range (figure 5(a)). A similar phenomenon is found with the selection of the 90 nm air gap. At a given wavelength, the absorptance as a function of the air layer thickness exhibits peaks associated with the Fabry–Perot resonances of the structure (figure 5(b)). Again, this particular thickness is selected due to the fact that a structure with a smaller air gap possesses smaller absorptance in the visible range (figure 5(b)). We note that the enhancement factor Q as a

Table 1. Enhancement factor Q of the optimized TA and TSiC structures of figure 2. The reference point is a tungsten structure.

Structure	Q
TA	1.929
Reduced TA	1.929
TSiC	1.853
Reduced TSiC	1.849

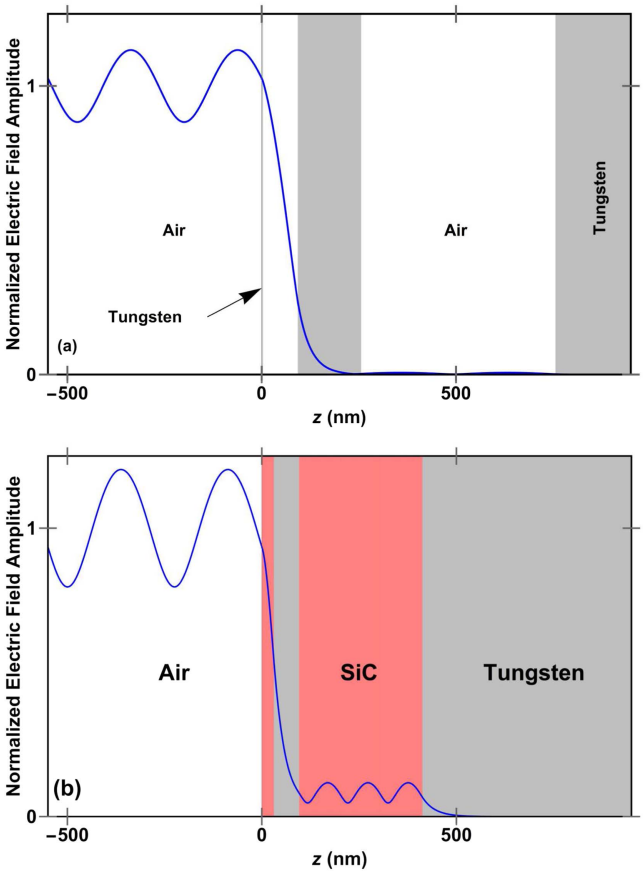

Figure 4. Profile of the electric field amplitude, normalized with respect to the field amplitude of the incident plane wave for the TA and TSiC optimized structures described in figure 2. The structures are excited by a normally incident plane wave at the wavelength of $\lambda = 550$ nm, near the center of the visible wavelength range. (a) For the TA structure, the ratio of the power absorbed inside each layer to the total power absorbed in the structure was calculated and from left to right, beginning with tungsten, is: {0.79, 0, 0.21, 0, 0}. That is, ∼79% of the power is absorbed in the first tungsten layer adjacent to air. (b) For the TSiC aperiodic structure, the thickness of the first tungsten layer is zero; thus, the layer adjacent to air is silicon carbide. The ratio of the power absorbed inside each layer to the total power absorbed in the structure from left to right, beginning with SiC, is: {0, 0.99, 0, 0.01}. That is, ∼99% of the power is absorbed in the first tungsten layer.

function of the air-gap thickness exhibits additional peaks. However, the maximum enhancement is obtained at the first peak, since for higher-order peaks the absorptance is not high in the entire visible band (figure 5(b)).

In addition, it turns out that the air layer with 500 nm thickness above the substrate (figure 4(a)) is not critical in the optimized TA structure, since, if this layer is removed, the absorptance at normal incidence in the visible is only reduced by up to ∼0.5% (figure 6(a)). Based on this, we may conclude that in practice the optimized TA structure is equivalent to a tungsten layer with 3.4 nm thickness which is separated by an air layer with 90 nm thickness from the tungsten substrate. We will henceforth refer to a structure consisting of a thin tungsten layer and an air layer on top of a tungsten substrate (figure 7) as the reduced TA structure.

We note that, for a thin metallic film placed $\lambda/4$ away from a perfect mirror, the required film thickness d_1 in order to achieve perfect impedance matching and therefore complete absorption in the film for normal incidence is [26]

$$d_1 = \frac{\lambda}{4\pi nk}, \tag{4}$$

where n and k are the real and imaginary part of the refractive index of the metal, and λ is the wavelength. In the reduced TA structure, figure 6(a), the tungsten substrate is not a perfect mirror, and the thickness of the air gap above the substrate is not exactly $\lambda/4$ in the visible band. In addition, the optimized TA structure was obtained by optimizing the structure in the whole visible band rather than at a single wavelength. Despite these differences, we find that equation (4) approximately predicts the thin tungsten layer thickness in the optimized TA structure. More specifically, the required tungsten film thickness d_1, obtained from equation (4) in the visible range, is 3.9 nm $\leqslant d_1 \leqslant$ 5.5 nm, which is roughly the actual optimized layer thickness of 3.4 nm (figure 2). We note that, while the index of refraction of tungsten is wavelength-dependent, and thus the optimum layer thickness is also wavelength-dependent, this 3.4 nm thickness choice for the thin tungsten layer results in absorption in the layer of more than 73.5% over the entire visible band. It is also interesting to note that, as the wavelength λ increases, the nk product for tungsten in the visible also increases [16]. Thus, the required tungsten film thickness d_1, for complete absorption obtained from equation (4), is relatively constant in the visible band. This suggests that tungsten is a uniquely suited material for thin-film perfect absorbers in the visible.

Figure 4(b) shows the electric field amplitude profile for the optimized TSiC structure. The field amplitude is normalized with respect to the incident plane wave field amplitude. The plane wave is normally incident and has a wavelength of $\lambda = 550$ nm. The reflectance of the TSiC structure is only ∼10%, since almost perfect impedance matching between the structure and air is achieved. Additionally, the field in the structure is not enhanced. Therefore, similar to the TA structures, the high absorptance is not due to strong resonances; in other words, the quality factor of the resonances is low. This is in agreement with the broadband and broad-angle absorptance of the structure (figure 3(c)).

However, we note that, compared to the TA structures, there are differences in the mechanisms that cause high

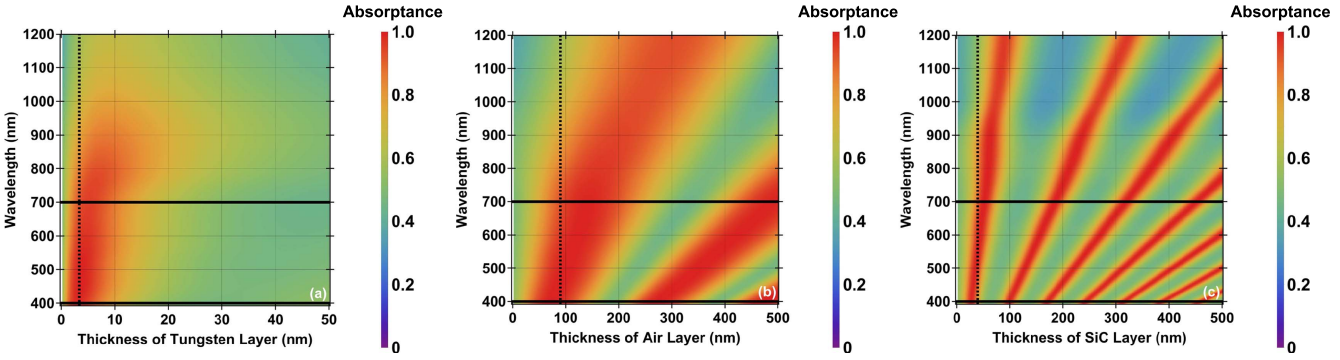

Figure 5. (a) Absorptance in the normal direction of a four-layer TA structure (figure 1) as a function of wavelength and the thickness of the first tungsten layer adjacent to air. All other layer thicknesses are as in the optimized TA structure described in figure 2. (b) Absorptance in the normal direction of a four-layer TA structure (figure 1) as a function of wavelength and the thickness of the air layer below the first tungsten layer. All other layer thicknesses are as in the optimized TA structure described in figure 2. (c) Absorptance in the normal direction of a three-layer TSiC structure (figure 1) as a function of wavelength and the thickness of the first silicon carbide layer adjacent to air. All other layer thicknesses are as in the optimized TSiC structure described in figure 2. The horizontal, thick, black lines show the visible wavelength range, while the dashed vertical line denotes the optimized structure dimension.

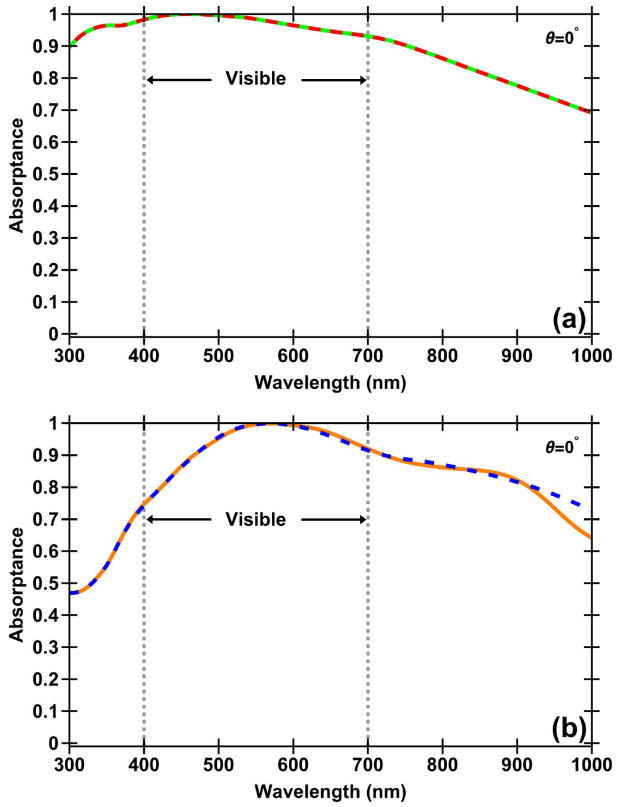

Figure 6. (a) Comparison of the absorptance spectra in the normal direction of the optimized TA structure described in figure 2 (solid line) and the reduced TA structure, which consists only of two layers (dashed line): a thin tungsten layer and an air gap above a thick tungsten substrate (figure 7). The thicknesses of the two layers of the reduced TA structure are the same as the thicknesses of the first two layers of the optimized TA structure. (b) Comparison of the absorptance spectra in the normal direction of the optimized TSiC structure described in figure 2 (solid line) to the reduced TSiC structure which consists of a silicon carbide layer above a thick tungsten substrate (dashed line). The thickness of the silicon carbide layer of the reduced TSiC structure is the same as the thickness of the first silicon carbide layer of the optimized TSiC structure.

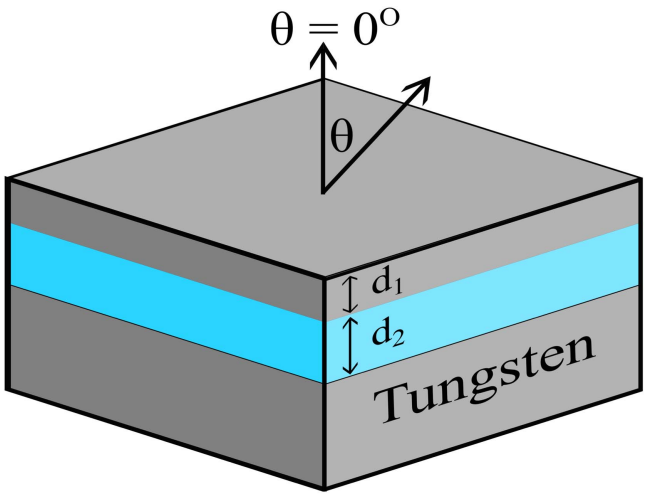

Figure 7. Schematic of the reduced structure. It consists of a single layer of tungsten and a dielectric layer above a semi-infinite tungsten substrate.

absorptance in the visible range. In contrast to the TA structures, in which the optimized structure possessed a thin tungsten layer that absorbed an overwhelming majority of incident light in the visible wavelength range, the tungsten layer thickness, which borders air in the TSiC structure, was optimized to be zero (figure 2). As a result, in the TSiC case, equation (4) is irrelevant. In figure 5(c), we show the absorptance of the TSiC structure as a function of wavelength and the thickness of the silicon carbide layer adjacent to air. As in the TA case, at a given wavelength, the absorptance as a function of the silicon carbide layer thickness exhibits peaks associated with Fabry–Perot resonances of the structure (figure 5(c)). As before, the optimum layer thickness is selected based on the fact that a structure with a smaller thickness possesses smaller absorptance in the visible (figure 5(c)). In addition, as in the TA case, the enhancement

factor Q as a function of the silicon carbide layer thickness exhibits additional peaks, but the maximum enhancement is obtained at the first peak, since for higher order peaks the absorptance is not high in the entire visible band (figure 5(c)).

We also investigated the effect of changing the thickness of the tungsten layer below the silicon carbide layer next to air, and found that, as long as this layer thickness is larger than 60 nm, the absorption of the structure is unchanged. Based on this, we investigated the properties of a reduced TSiC structure, which consists of a single silicon carbide layer above a thick tungsten substrate. The thickness of the silicon carbide layer of the reduced TSiC structure is the same as the thickness of the first silicon carbide layer of the optimized three-layer TSiC structure (39 nm). We found that for the reduced TSiC structure, the absorptance at normal incidence in the visible range is only reduced by up to ~0.5%, compared to the optimized TSiC structure (figure 6(b)). We note, however, that the absorptance changes by approximately 10% in some regions of the near-infrared wavelength range (figure 6(b)).

A single silicon carbide layer can lead to high absorptance in the whole visible wavelength range, because such a layer can provide near-perfect impedance matching between air and the tungsten substrate. More specifically, the impedance η_{TSiC} of the reduced TSiC structure, which consists of a silicon carbide layer above a thick tungsten substrate, is

$$\eta_{\mathrm{TSiC}} = \eta_{\mathrm{SiC}} \frac{\eta_{\mathrm{W}} + i\eta_{\mathrm{SiC}} \tan(\beta_{\mathrm{SiC}} d_2)}{\eta_{\mathrm{SiC}} + i\eta_{\mathrm{W}} \tan(\beta_{\mathrm{SiC}} d_2)}, \tag{5}$$

where η_{W} and η_{SiC} are the impedance of tungsten and silicon carbide, respectively, $\beta_{\mathrm{SiC}} = 2\pi n_{\mathrm{SiC}}/\lambda$, n_{SiC} is the refractive index of silicon carbide and d_2 is the thickness of the silicon carbide layer. As an example, using equation (5) for $\lambda = 570$ nm, we find $\eta_{\mathrm{TSiC}} = 356.3 + 3.4i\ \Omega$, which is very close to the air impedance $\eta_{\mathrm{air}} = 377\ \Omega$.

As mentioned above, we found that the optimized TA structure (figure 2) is essentially equivalent to the reduced TA structure consisting of a thin tungsten layer and an air layer above a thick tungsten substrate (figure 7). Similarly, the optimized TSiC structure (figure 2) is essentially equivalent to a reduced TSiC structure, which consists of a single silicon carbide layer above a thick tungsten substrate. In an effort to provide a unified description of the TA and TSiC structures, we investigate the optimum thickness of the tungsten and dielectric layers as a function of the refractive index of the dielectric layer n for the structure of figure 7. For simplicity, the structure is optimized to maximize the absorptance at a single wavelength of $\lambda = 550$ nm. For $n = 1$ (air), the optimum thickness of the tungsten layer was found to be 3.9 nm. Note that this thickness is slightly different than the optimized value of 3.4 nm in figure 2, since here we optimize the structure at a single wavelength rather than in the whole visible wavelength range. As n is increased, the optimum tungsten layer thickness decreases and becomes zero for $n \geqslant 2.6$ (figure 8(a)). Thus, for lower refractive indices n, the presence of a thin tungsten layer, which absorbs most of the incident light, is beneficial. For higher refractive indices, the thin tungsten layer is not required, since the single dielectric layer can provide near-perfect impedance matching between air and the tungsten substrate. In this case, the incident light is mostly absorbed in the tungsten substrate. Silicon carbide has an index of refraction of $2.62 \leqslant n \leqslant 2.77$ over the visible wavelength range, and thus a single silicon carbide layer can provide near-perfect impedance matching, without the presence of a thin metallic absorbing layer. For the dielectric layer, as expected, as the refractive index n increases, the optimum thickness of the layer decreases (figure 8(b)).

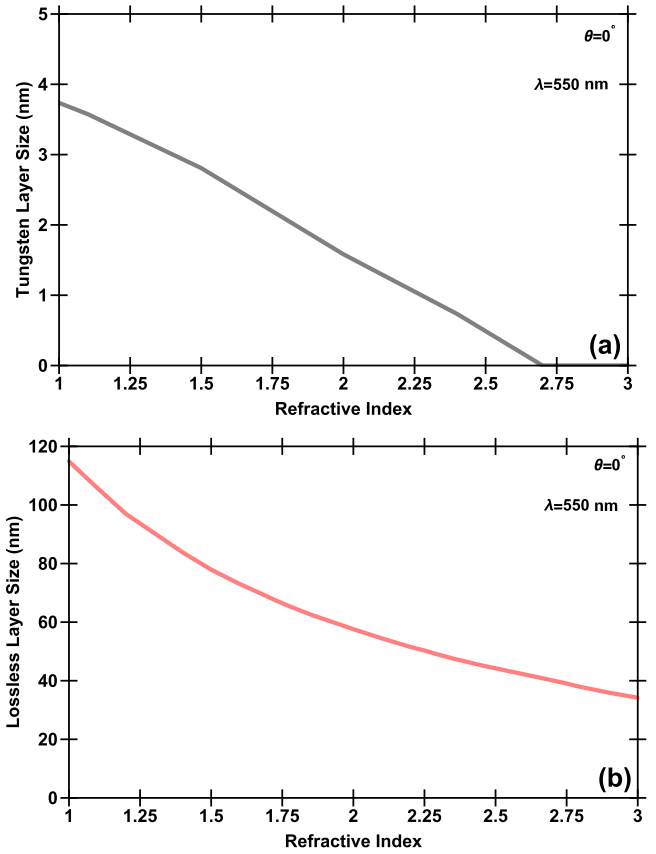

Figure 8. (a) Optimum thickness of the tungsten layer d_1 as a function of the refractive index of the dielectric layer n for the structure of figure 7. The structure is optimized to maximize the absorptance in the normal direction at the wavelength of $\lambda = 550$ nm. (b) Optimum thickness of the dielectric layer d_2 as a function of the refractive index of the dielectric n for the structure of figure 7. The structure is optimized to maximize the absorptance in the normal direction at the wavelength of $\lambda = 550$ nm.

4. Conclusion

In this paper, we designed broadband visible absorbers. We considered structures composed of TA or TSiC multilayer stacks of varying aperiodic thicknesses on tungsten substrate. We used a hybrid optimization method, which includes a micro-genetic global optimization method and a local optimization method to maximize the absorptance of these structures in the visible.

Both the TA and TSiC optimized structures that we obtained using this process show drastically improved absorptance in the visible range, in comparison to tungsten. When optimized, these structures exhibit absorptance which approaches unity. We achieved almost perfect impedance matching between these structures and air. Additionally, no field enhancement was observed. Thus, the high absorptance is not related to resonances with high quality factors, which is in agreement with the broadband and broad-angle absorptance of our structures.

We also found that the TA structure obtained through optimization is essentially equivalent to a reduced TA structure consisting of a thin tungsten layer and an air layer above a thick tungsten substrate. Similarly, we found that the optimized TSiC structure is essentially equivalent to a reduced TSiC structure, which consists of a single silicon carbide layer above a thick tungsten substrate. In this case, the single silicon carbide layer leads to high absorptance in the whole visible wavelength range, because it provides near-perfect impedance matching between air and the tungsten substrate.

As final remarks, we note that, due to the high melting temperature of tungsten and silicon carbide, the proposed aperiodic absorbers can also be used in thermal emitter applications.

Acknowledgments

This research was supported by the National Science Foundation (Award Nos. 1102301, 1254934, 1263236, 0968895), and a Fund for Innovation in Engineering Research (FIER) grant from the Louisiana State University College of Engineering. C You would like to acknowledge support from an Economic Development Assistantship from the Louisiana State University System Board of Regents. J P Dowling wishes to also acknowledge support from the Air Force Office of Scientific Research, the Army Research Office, and the Northrop Grumman Corporation.

ORCID iDs

Chenglong You https://orcid.org/0000-0002-1383-0551

References

[1] Rephaeli E and Fan S 2009 *Opt. Express* **17** 15145–59
[2] Čelanović I, O'Sullivan F, Ilak M, Kassakian J and Perreault D 2004 *Opt. Lett.* **29** 863–5
[3] Florescu M, Lee H, Puscasu I, Pralle M, Florescu L, Ting D Z and Dowling J P 2007 *Sol. Energy Mater. Sol. Cells* **91** 1599–610
[4] Cui Y, He Y, Jin Y, Ding F, Yang L, Ye Y, Zhong S, Lin Y and He S 2014 *Laser & Photon. Rev.* **8** 495–520
[5] Polman A and Atwater H A 2012 *Nat. Mater.* **11** 174–7
[6] Hägglund C, Zeltzer G, Ruiz R, Thomann I, Lee H, Brongersma M L and Bent S F 2013 *Nano Lett.* **13** 3352–7
[7] Deng H, Li Z, Stan L, Rosenmann D, Czaplewski D, Gao J and Yang X 2015 *Opt. Lett.* **40** 2592–5
[8] Park J, Kim S J and Brongersma M L 2015 *Opt. Lett.* **40** 1960–3
[9] Yu J, Shen Y, Liu X, Fu R, Zi J and Zhu Z 2004 *J. Phys.: Condens. Matter* **16** L51
[10] Cortes C L, Newman W, Molesky S and Jacob Z 2012 *J. Opt.* **14** 063001
[11] Drachev V P, Podolskiy V A and Kildishev A V 2013 *Opt. Express* **21** 15048–64
[12] Cui Y, Fung K, Xu J, Ma H, Jin Y, He S and Fang N X 2012 *Nano Lett.* **12** 1443–7
[13] Lee B J and Zhang Z M 2006 *J. Appl. Phys.* **100** 063529
[14] Granier C H, Lorenzo S G, Dowling J P and Veronis G 2015 *Proc. SPIE* **9546** 954603
[15] Cornelius C M and Dowling J P 1999 *Phys. Rev.* A **59** 4736–46
[16] Lide D R 1998 *CRC Handbook of Chemistry and Physics* (Boca Raton, FL: Taylor & Francis)
[17] Krishnakumar K 1990 *Proc. SPIE* **1196** 289–96
[18] Goldberg D E and Deb K 1991 *Foundations of Genetic Algorithms* ed G J E Rawlins vol 1 (San Mateo, CA: Morgan Kaufmann) pp 69–93
[19] Deb K and Agrawal S 1999 *Foundations of Genetic Algorithms* ed W Banzhaf and C Reeves vol 5 (San Francisco, CA: Morgan Kaufmann) pp 265–86
[20] Goldberg D E, Deb K and Clark J H 1992 *Complex Syst.* **6** 333–62
[21] Johnson J M and Samii Y R 1996 *IEEE Antennas Propagat. Soc. Int. Symp.* pp 1480–3
[22] Granier C H, Afzal F O, Min C, Dowling J P and Veronis G 2014 *J. Opt. Soc. Am.* B **31** 1316
[23] Granier C H, Afzal F O, Lorenzo S G, Reyes M, Dowling J P and Veronis G 2014 *J. Appl. Phys.* **116** 243101
[24] Johnson S G 2014 The NLopt Nonlinear-Optimization Package http://ab-initio.mit.edu/nlopt
[25] Powell M J D 1994 *Advances in Optimization and Numerical Analysis* ed S Gomez and Hennart J-P (Berlin: Springer) pp 51–67
[26] Biener G, Niv A, Kleiner V and Hasman E 2007 *Opt. Lett.* **32** 994